Diego Arosio · Laura Longoni · Monica Papini · Grégory Bièvre · Luigi Zanzi

# Geological and geophysical investigations to analyse a lateral spreading phenomenon: the case study of *Torrioni di Rialba,* northern Italy

**Abstract** We combined geological, geomechanical, geophysical and remote sensing investigations, including persistent scatterer interferometry and bathymetry, to study a slope where four conglomerate towers laterally spread over a shale layer. Electrical resistivity tomography surveys confirm a shale layer that underlies the rock towers with an attitude parallel to the slope. Field mapping reveals that the stability of the rock towers is threatened by weakly cemented conglomerate layers, large eroded zones and karstic weathering due to water circulation. We deem that the most probable failure mechanism would be the toppling of the southernmost tower, promoted primarily by the weak conglomerate layer in its lower section. The plastic shale layer underneath the rock cliff is very likely to promote lateral spreading that may have triggered the toppling of an additional former rock pillar, whose rock blocks were found in the lake during a bathymetric survey. Close- and long-range remote sensing of displacements provide no results that could be interpreted with confidence. Seismic noise recording sessions with 3C low-frequency velocimeters suggest that the dynamic conditions of the towers do not show appreciable variations across the recording sessions, especially considering the two rock towers featuring the most interesting spectral characteristics. However, both the resonance frequencies and the preferential oscillation directions estimated from the seismic noise datasets are consistent with the analytical relationships and will support the design of an effective monitoring strategy.

**Keywords** Lateral spreading · Seismic noise · Electrical resistivity tomography · Shale · Rock toppling

## Introduction

Several definitions of lateral spreading phenomena have been proposed in the scientific literature and a recent update of Varnes landslide classification identified three main classes of spreading involving (i) rock slope spread, (ii) sand/silt liquefaction spread and (iii) sensitive clay spread (Hungr et al. 2014). Generally, the term rock spreading refers to mass movements that occur on slopes consisting of rigid blocks of stronger rock placed over soft plastic formations (Pasuto and Soldati 1996). However, a more accurate classification should take into account the features of the surface of rupture. According to Hungr et al. (2014), spread refers to slopes where a large and well-defined surface of movement may be identified, compound slide involves the presence of either a shear plane or a thin shear band and deformation assumes a gradual increase in plastic straining with depth. The latter class is generally referred to as deep-seated gravitational slope deformation (DSGSD), and can be further subdivided in sackung and lateral spreading. The former refers to sagging of high and steep slopes, whilst the latter describes a lateral expansion of rock masses along a shear plane. Although rock spreading is usually associated to slow displacement rates, it may evolve into faster movements such as sliding, toppling or rock fall. Accordingly, detailed assessment and careful monitoring strategies should be taken into account for hazard mitigation when dealing with such phenomena (Soldati 2013).

Numerous lateral spreading phenomena have been observed in Italy (Soldati and Pasuto 1991; Carobene and Cevasco 2011; Viero et al. 2010), with the majority located in the northern Apennines (Chelli et al. 2006; Picarelli and Russo 2004; Spreafico et al. 2016; Spreafico et al. 2017). However, very few case studies have been thoroughly investigated and adequately documented (Pasuto and Soldati 2013), despite the risks potentially associated with such mass movements. This is mainly because detailed assessment of the geological conditions and parameters concerning this class of landslides is rarely straightforward. Nonetheless, defining geological conditions accurately as possible is crucial to model the kinematic and dynamic behaviour of an investigated slope, to identify possible triggering factors and to properly address risk analyses.

The work presented here regards the pre-Alpine area in the Southern-Central Alps (Fig. 1). Here, Alpine orogenic processes have produced very complex lithological and structural conditions, featuring several faulted and overthrusted tectonic units (Laubscher 1985; Gianotti and Perotti 1986). The peculiar geological history of this area results in a large number of mass movements of different types and sizes. According to the national landslides database (IFFI 2018), these active features have been classified as DSGSDs, rockfalls, flows and slides. Although lateral spreading phenomena seldom occur in this area, in this study we focus on a slope that may be affected by such a mass movement. Of concern are two distinctive features observed on the slope: four rock pillars separated by very persistent vertical fractures and a shale outcrop (i.e. plastic material) mapped close to the base of the pillars. The geological uniqueness of this case study is especially pertinent given the vulnerability of infrastructure including a national highway and railway line at the base of this slope.

In this context, we present a multi-disciplinary approach involving geological, geomorphological and geophysical investigations, together with remote sensing analyses, with the final aim of producing an engineering-geological model of the slope under investigation. Indeed, the integration of datasets obtained from different techniques can be used to limit ambiguities related to the knowledge of complex geological settings (Booth et al. 2015). After a general description of the case study and of the geological setting, we focus on the field surveys. Conventional methodologies, such as classical geological and geomorphological mapping, logging of boreholes, satellite interferometry and geoelectrical surveys, have been combined with less standard techniques, including bathymetry and seismic noise recording sessions. Then,
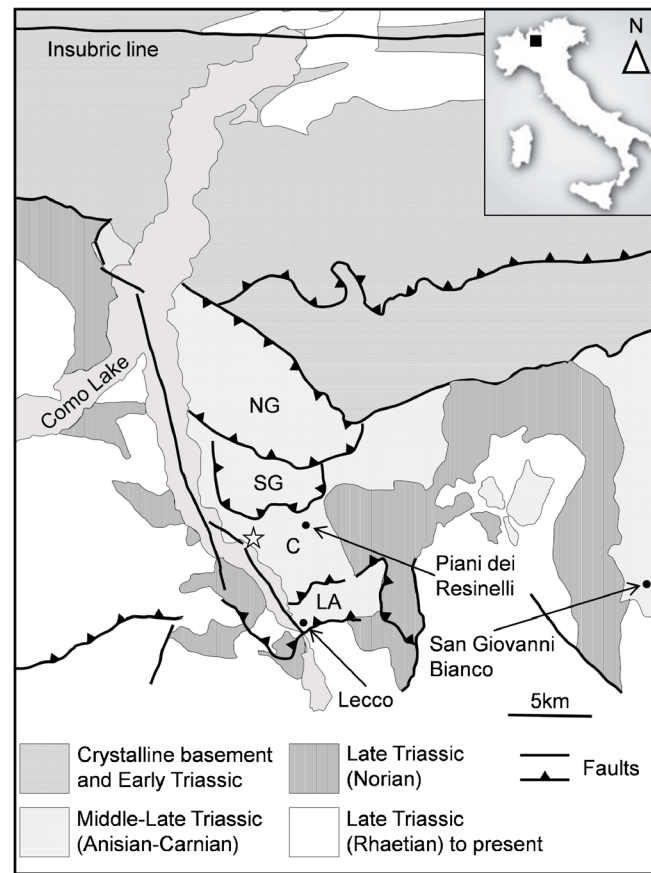
**Fig. 1** Geological setting south of the *Insubric line* (Southern-Central Alps) with some of the main structural units and lineaments. The star pinpoints the location of the *Torrioni di Rialba* site. NG, SG, C and LA indicate the Northern *Grigna*, Southern *Grigna*, *Coltignone* and *Lecco Autoctono* tectonic units, respectively. See text for details

we discuss the outcomes of our investigations with the aim of developing a suitable geological model that will serve as a starting point for future hazard and risk analyses. The results of this study can help to evaluate possible evolution of the stability conditions of the slope, to design and to plan the most promising monitoring activities and to estimate the size of possible collapses and the associated scenarios.

**Case study:** *Torrioni di Rialba*

The *Torrioni di Rialba* are four rock towers with subvertical walls up to 100 m high, located 5 km northeast of the city of Lecco, northern Italy (Fig. 1). The stability of these rock pillars (hereafter numbered from 1 to 4 from the southernmost; Fig. 2) is of utmost importance since they are located approximately 200 m upslope of the narrow corridor where important lifelines, such as a national highway, a railway line and electric power lines, run adjacent to each other and connect the northern part of the region with its 200,000 inhabitants to major infrastructure in the Po Plain. In addition, a small hydroelectric power plant located on the lake shore near the transportation infrastructure and collects water from a pipe running downslope just east of the towers (Fig. 2a).

Monitoring activities were carried out between 2004 and 2005 using 16 extensometers deployed across the main fractures

separating the towers and 7 prism reflectors bolted on the south face of the southernmost tower to be used when surveying with a total station theodolite. Over 12 months, no significant displacements were detected and monitoring stopped because of the lack of further financial support. Nevertheless, in the last decade numerous small rock collapses (< 0.5 m$^3$) have been reported and, considering both the geological and the geomorphological settings of the site, brittle failure of one or more rock pillars could occur with no significant precursory signals. A potentially catastrophic consequence of a slope failure would be the generation of a tsunami if rock blocks entered the lake. On these grounds, it is extremely important to deepen our knowledge about the nature of the slope and to develop a physical model as accurate to better define reasonable risk scenarios and interpret with confidence subtle changes in monitoring activities.

**Geological setting**

*Torrioni di Rialba* are located in the western section of the Southern-Central Alps, approximately 30 km south of the Periadriactic Seam that is often referred to as *Insubric line* in this area (Fig. 1). This line marks the collision between the Eurasian and the Adriatic tectonic plates, and thus delineates a continent-to-continent convergent boundary causing transpression, folding and uplifting of plate edges.
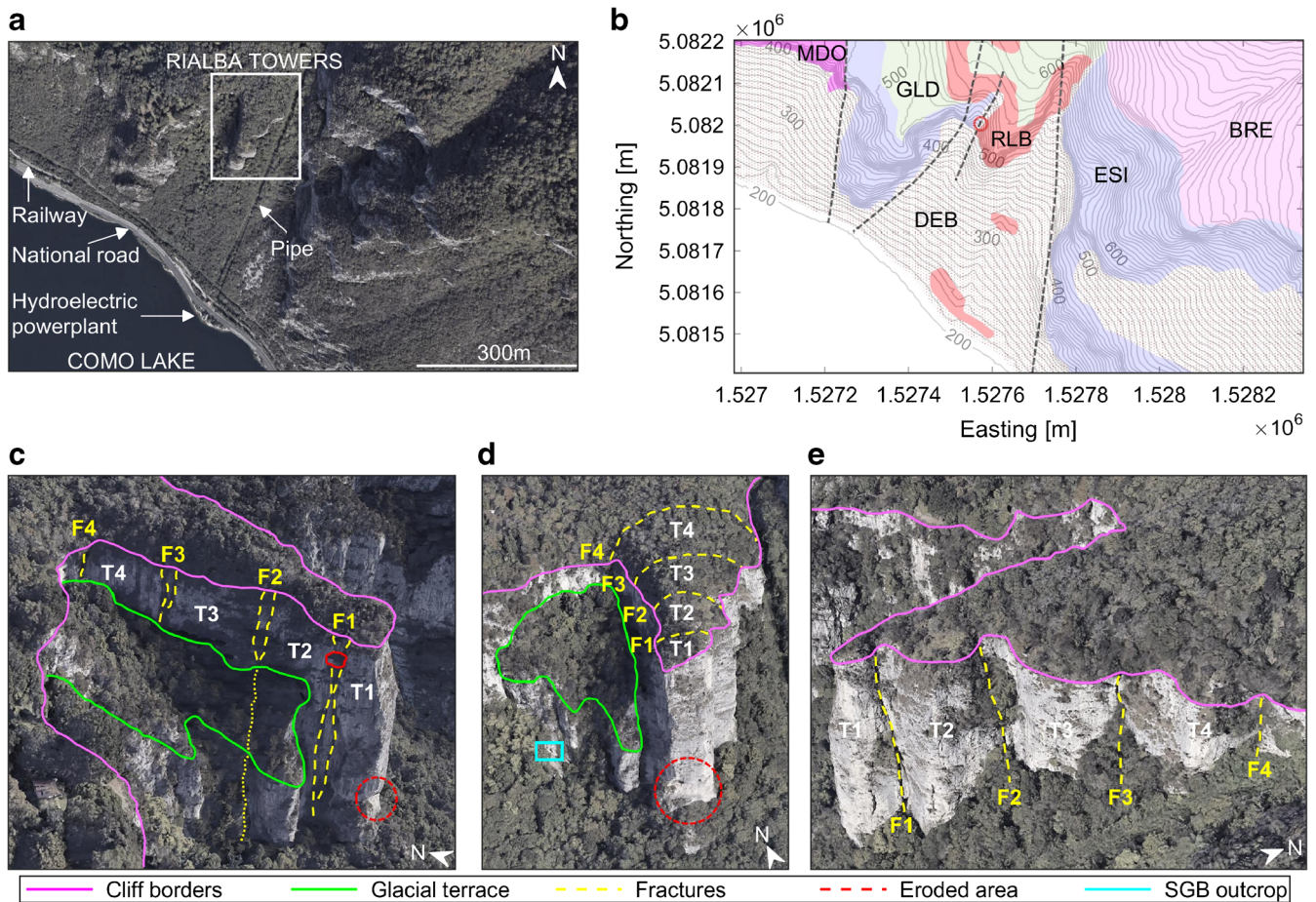
**Fig. 2** **a** Plan view of the *Rialba* Towers area. **b** Geological map with the main formations: RLB *Rialba* conglomerate, ESI *Esino* limestone, BRE *Breno* limestone, MDO main dolomite, GLD glacial deposits, DEB slope debris. Red circle marks the known outcrop of *San Giovanni Bianco* shale and dashed black lines are faults. **c** Northwest, **d** south, and **e** southeast view of the *Rialba* Towers. See text for details

The lithological and structural complexity of the area is related to different depositional events and deformation episodes connected to the Alpine orogeny. The resulting geological structure consists of a series of tectonic units, variously faulted and overthrusted that place different stratigraphic units in close contact with one another (Laubscher 1985; Gianotti and Perotti 1986). In more detail, *Torrioni di Rialba* belongs to the *Grigne* massif, whose main tectonic units are Northern *Grigna*, Southern *Grigna*, *Coltignone* and *Lecco Autoctono*, respectively, from north to south (Fig. 1). These units are separated by major thrusts along the E-W direction caused by transpressive stresses along the N-S direction that generated further faults and fractures E-W trending. Moreover, there is another important fault system along the perpendicular direction (N-S).

*Torrioni di Rialba* are made of a formation named *Rialba* conglomerate that is essentially a carbonate surface deposit consisting of (i) very well cemented and weakly karstified diamictite containing variously sized sharp-edged clasts (of which up to 25% are gravel-sized) and (ii) local pebbles embedded in both yellow and reddish sandstones. Bedding is generally poorly discernible and the formation is typically divided into rock blocks that can be observed both at the base and at the top of the towers.

The *Rialba* conglomerate sometimes includes boulders of considerable size (up to a few cubic meters) and, in the top part of the towers, layers generally feature smaller size particles, but still very well cemented. The degree of cementation is usually linked to the age of the deposit, the older one being extremely compact and competent.

The outcrop area of the *Rialba* conglomerate is rather small since this formation has been found only in this study site (Fig. 2b); this fact may support the hypothesis that the formation could be related to large landslides that affected the area between the late Miocene and Pliocene epochs. According to this assumption, a very large slope failure was promoted by two different tectonic events (Bini et al. 2004). First, the displacement of Lecco's fault resulted in the formation of Como Lake (Fig. 1), which in turn produced unstable slope conditions. Second, the cessation of interaction between the Mediterranean Sea and the Atlantic Ocean caused the water level in the Mediterranean Sea to decrease. This subsequently caused an increase in the erosive activity of the rivers, with the creation of very steep and deep canyons that further undermined slope stability in the valleys surrounding Como Lake. According to Bini et al. (2004), in the late Miocene epoch, a rock collapse occurred in the area of *Piani*

*dei Resinelli* (Fig. 1) and failed south-westwards into the lake. This rock failure produced very chaotic detritus that later lithified into the *Rialba* conglomerate.

*Rialba* conglomerate is bounded both to the east and to the west by *Esino* limestone (late Anisian–Ladinian; Fig. 2b), a formation resulting from a carbonate platform and consisting of massive layers of limestone, grey dolomitic limestone and dolomite, whose thicknesses range from 250 to 800 m. The upper limit of *Rialba* conglomerate is at the top of the towers and consists of an erosional plane over which glacial deposits can be found (Fig. 2b). The existence of a glacier in a former epoch is supported by the presence of glacial erratics completely different from the site lithology on the erosional plane (Fig. 3e). Furthermore, a glacial terrace northwest of the towers (Fig. 2) confirms erosion, transport and sedimentation activities promoted by the glacier during the Quaternary epoch.
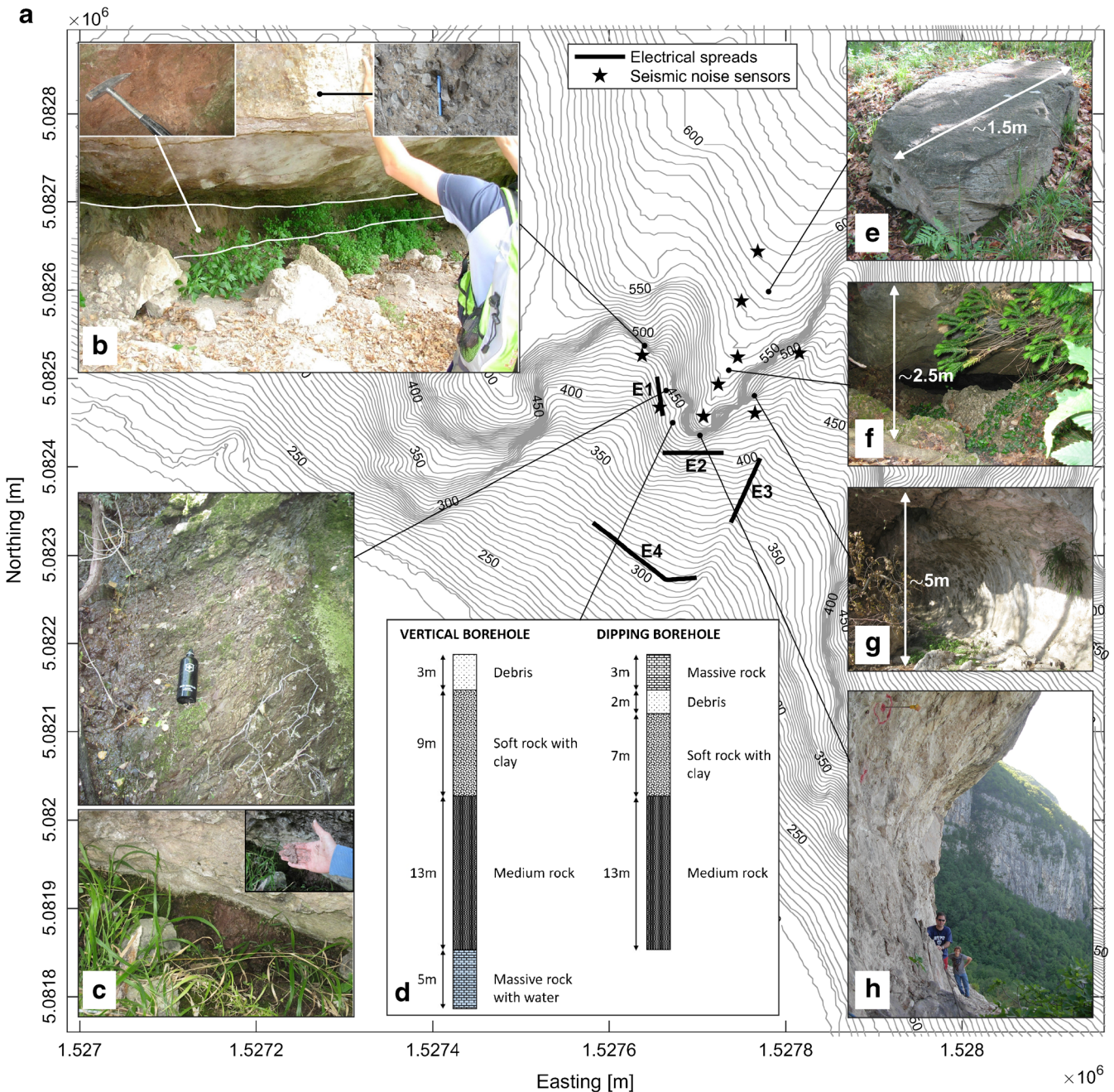


Fig. 3 **a** Topographic map of the investigated area with locations of electrical and seismic noise surveys. **b** Cave with the previously known outcrop of *San Giovanni Bianco* formation; white solid lines bound the outcrop and inlets show *Rialba* conglomerate and *San Giovanni Bianco* shale (top right and top left, respectively). **c** Springs found at the base of the glacial terrace with *San Giovanni Bianco* outcrops. **d** Boreholes performed at the base of tower 1. **e** One of the glacial erratics found on the top of the Rialba towers. **f** Top view of fracture F2. **g** One of the erosional caves found at the base of the towers. **h** Side view of the eroded cavity in the lower section of tower 1

The lower limit of *Rialba* conglomerate is supposed to be a layer whose formation and attitude are still under debate. The only information available thus far is related to area section at the base of the glacial terrace northwest of the towers, at an elevation of about 440 m. Here, water erosion has created a cave approximately 20 m wide having a roof with weakly cemented conglomerate and a floor with an outcrop of reddish shale belonging to the *San Giovanni Bianco* formation (Fig. 3b). The formation is named after the town of *San Giovanni Bianco* in the *Brembana* valley (Fig. 1), about 25 km east of the study site, where the type locality has a moderate extent. Elsewhere, the *San Giovanni Bianco* formation is never entirely preserved, as it constitutes a preferential path along which tectonic displacements took place. Actually, together with the underlying *Gorno* formation, it is the tectonic horizon that promoted thrust faulting of the abovementioned *Coltignone* and southern *Grigna* structural units (Fig. 1). In the type locality, the *San Giovanni Bianco* formation is about 200 m thick, whilst in other locations its thickness is deemed to be around 120–160 m, although the tectonic erosion prevents any accurate thickness estimation. Because of the genesis of *Rialba* conglomerate we discussed earlier, the boundary between *San Giovanni Bianco* and *Rialba* conglomerate cannot be associated to any stratigraphic sequence.

This formation is evidence of the considerable retreat of seawater during the late Carnian age, and development of large coastal lagoons, in which fine clayey sediments were deposited. Because of the evaporation of seawater, salt lenses are often found within shale. The formation is heterogeneous, as it consists of successions of sandstones, mudstones, dolomite and, more rarely, limestone. The base of the formation is characterised by the presence of medium-to-coarse grey sandstones. In the study area, the different zones are poorly differentiated and the unit is predominantly represented by sandstones, siltstones and reddish shale.

In the following pages, we describe all the investigations undertaken to improve our knowledge related to the physical model and the stability of the slope. The *San Giovanni Bianco* formation outcrops in a very limited area below the glacial terrace northwest of the towers. Thus, we particularly focus on the trend and the thickness of this formation in the subsurface below the *Rialba* conglomerate. Because of the poor mechanical properties of *San Giovanni Bianco* formation with respect to the overlaying conglomerate towers, the outcomes of these investigations will contribute significantly to a better understanding of the dynamic and kinematic behaviour of the rock towers.

### Field surveys

#### Geological investigations

A very significant structural feature is the remarkable set of four parallel fractures that separates the conglomerate rock mass into four rock towers. These fractures (named F1 to F4 south to north; Fig. 2) have similar attitude, with dip direction ranging from 205° to 215° and dip close to 85°, linear persistence of about 90%. Apertures as large as 5 m can be observed on both the top and the sides of the rock mass; they have a linear trend on the south-eastern face where they can be tracked from the top to the bottom of the cliff. On the north-western face, they have more curved and complex trends where they can be observed in the top section because of the glacial terrace next to the cliff (Fig. 2c).

Fracture F1 starts at 535 m asl, where it is about 25 m from the southernmost tip of the towers and is filled with organic soil. On the south eastern face, the fracture runs straight for about 100 m and at the base is 4 m wide and filled with weakly cemented conglomerate blocks. This is the only major fracture that can be observed on the north-western face along its whole length, where it is divided into two subparallel fractures a few meters apart (Fig. 2c). Figure 2c also highlights the presence of a rock block with an estimated volume of about 150 m³, stuck in the upper section of the fracture. Fracture F2 is about 2 m wide and starts at about 545 m asl; it is the only fracture that, on the top plane at least, is completely open so that it is possible to observe the characteristics of the two sides of the fracture (Fig. 3f). This fracture is about 80 m long and in its top part it is divided into two segments that isolate an overhanging section. Fracture F3 starts at about 555 m asl and is about 70 m long. Lastly, F4 at the top is at 575 m asl, is about 2–3 m wide, and it is possible to track the fracture on the whole south-eastern face of the towers for approximately 60 m. Table 1 lists the overestimated sizes and volumes of the four pillars, approximated as right rectangular prisms, separated by the main discontinuities.

Besides the main fracture set described above, two minor sets of discontinuities have been surveyed. Both sets have similar mean parameters, consisting of apertures around 5 mm, spacing of 0.4 m, linear persistence below 50% and cracks generally infilled with colluviated material (sand and soil). On the other hand, they have different attitudes: one set having an attitude 330°/85°, whilst the other an orientation of 260°/85°.

To complete the geomechanical classification of *Torrioni di Rialba*, we performed tests with a Schmidt hammer on different outcrops. However, this test was not suitable for plastic materials, i.e. *San Giovanni Bianco*, as they yield very low hammer rebound values ($R_N$). For each tested outcrop, we set a survey grid of 12 points, averaged over 6 measurements to limit the errors due to non-perfectly planar surface. We also considered sections with intact and well-confined rock, in addition to two areas of *Rialba* conglomerate with different degrees of cementation (i.e. fairly and well cemented) to evaluate the influence of this parameter on the rock properties.

Table 2 lists the mean values and standard deviations obtained with the Schmidt hammer, together with the mean uniaxial compression strength ($\sigma_{UCS}$), the mean tangent Young's modulus ($E_t$) at 50% of $\sigma_{UCS}$ and the mean seismic P wave velocity ($V_P$) estimated according to their empirical relationships with the rebound values (Katz et al. 2000; Aydin and Basu 2005; Sharma et al. 2011). Rebound values obtained for the conglomerate have larger standard deviations due to heterogeneity of the material, consisting of clasts with different sizes. The values reported in Table 2 increase

**Table 1** Geometrical parameters of the rock towers (approximated as right rectangular prisms)

| Tower | Size ($L \times W \times H$) (m) | Volume (m³) |
|---|---|---|
| 1 | $48 \times 30 \times 100$ | 144,000 |
| 2 | $66 \times 36 \times 80$ | 190,080 |
| 3 | $82 \times 38 \times 75$ | 233,700 |
| 4 | $100 \times 45 \times 65$ | 292,500 |

**Table 2** Geomechanical parameters of the formations in the investigated area derived from Schmidt hammer tests

| Rock formation | $R_N$ | $\overline{\sigma}_{UCS}$ (MPa) | $\overline{E}_t$ (GPa) | $\overline{V}_P$ (m/s) |
|---|---|---|---|---|
| *San Giovanni Bianco* shale | $16.7 \pm 1.7$ | 7.2 | 0.8 | 1500 |
| *Rialba* conglomerate (fairly cemented) | $43.4 \pm 4.0$ | 48.0 | 15.3 | 3030 |
| *Rialba* conglomerate (well cemented) | $53.9 \pm 3.1$ | 98.2 | 29.4 | 3980 |
| *Gorno* limestone | $47.6 \pm 8.8$ | 72.8 | 21.8 | 3440 |
| *Esino* limestone | $62.5 \pm 2.6$ | 178.2 | 46.3 | 4980 |

moving from the shale, through the conglomerate, to the limestone. As expected, *San Giovanni Bianco* formation has poor mechanical properties. We also surveyed a boulder of *Gorno* limestone, to characterise the formation that is the lower stratigraphic limit of the shale. Unfortunately, investigations with the Schmidt hammer were distorted by the rough rock surface and rebound values obtained show very large standard deviation (Table 2). However, the computed values fall within the ranges reported in the scientific literature for the investigated formations (e.g. Price 2009; Reynolds 2011).

In addition, we collected a few rock samples in the field to perform ultrasonic velocity measurements in the laboratory, and compared the results obtained with the empirical relationships and the Schmidt hammer. Tests performed with transducers at 150 kHz on samples whose water saturation was preserved gave comparable velocities, generally 10–15% higher. However, these values lack statistical significance and so are not reported in Table 2.

Regarding the hydrogeology of the investigated area, we envisage a deep water circulation supplied by rainfall events, runoff and infiltration from the main fractures, favoured by widespread rock mass fracturing and karst phenomena. We detected two minor springs with limited flow rate located at the base of the glacial terrace next to the north western side of the cliff. There is a spring at about 430 m asl associated with a 0.8-m-wide fracture that appears to be the extension of the fracture F2 that also affects the rock mass of the glacial terrace (Fig. 2c). Another spring can be found upslope at about 435 m asl. Close to both the springs, we observed several outcrops of reddish shale belonging to the *San Giovanni Bianco* formation (Fig. 3c) that seem to complement the only previously known outcrop in the cave at 440 m asl.

Groundwater springs at the base of *Torrioni di Rialba* support the presence of an impermeable layer extending underneath the rock mass, although the low permeability could be attributed to the presence of either the *San Giovanni Bianco* shale or the low-porosity *Gorno* limestone. The attitude of the shale layer mapped in the cave (14°/16°) does not match the original attitude because the layer has most probably been eroded by meteorological events, and catastrophic sliding of limestone blocks may have modified the older existing shale. This last point is also supported by the fact that the shale is a very brittle altered cataclastic layer. Similarly, the dip direction and dip of the cave roof, i.e. 90° and 30°, respectively, may not match the original attitude of the *San Giovanni Bianco* formation.

As a first attempt to determine the attitude of the shale layer within the investigated slope, we drilled two boreholes on the north-western side of tower 1, close to its base and not far from the shale outcrops (Fig. 3). Unfortunately, due to logistic constraints, we were forced to opt for rotary percussion drilling so that material identification was based solely on drilling cuttings and drilling speed. The first borehole was drilled vertically for 30 m, whilst the second one is 25 m deep and was drilled a few meters apart and is dipping 45° eastwards (i.e. it goes below tower 1). The vertical and dipping boreholes intersect soft rock with clay at 3-m and 5-m depth, for 9 m and 7 m, respectively (Fig. 3d), and a moderately harder material at greater depth. We believe the soft rock is associated with the *San Giovanni Bianco* formation, whilst the interpretation of the medium rock is more ambiguous. If the moderately stiffer rock is associated with the *Gorno* limestone underlying the shale, it may be that the shale layer has limited thickness, at least in the area westwards of tower 1.

Field investigations also revealed widespread rock weathering, promoted by both mechanical and chemical erosion, that generated several surface cavities and voids, especially at the foot of the pillars (Fig. 3g), and increases the risk of collapse of the towers by reducing their base areas. In the lower part of the southern face of tower 1, at about 450 m asl, there is a large eroded cavity (Figs. 2c, d and 3h) where we observed the presence of a weak layer consisting of very poorly cemented conglomerate that could influence the stability of the pillar.

With the purpose of better defining the risk scenarios related to the rock mass instability and of designing effective mitigation measures, it was decided to incorporate and analyse a high-resolution bathymetric survey of the coastal belt of Como Lake carried out by the provincial authority. Surprisingly, we noted the presence of large blocks in the lake in the area downslope the rock towers (Fig. 4a). Scuba divers have reported conglomerate rock blocks thousands of cubic meters in size and sediment thickness analysis of the mud deposited over the blocks dates emplacement of the blocks to the late middle ages. Therefore, we argue an additional pillar downslope of the present towers have failed in relatively recent historical times, and suggests that the massive collapse of one or more of the extant towers could occur.

Finally, taking advantage of available satellite radar acquisitions processed to obtain persistent scatterer interferometry (PSI) data (Costantini et al. 2009), we investigated possible slow displacements affecting the rock towers after monitoring with extensometers and prism reflectors ceased in 2005. Radar images collected by both ERS 1/2 and ENVISAT C-band satellites did not provide any useful PS points. In contrast, we were able to identify 12 PS in the datasets of the COSMO-SkyMed X-band radars within the time span of 3 years, from spring 2011 to spring 2014. The acquisition geometry of the satellites together with the geometry of the investigated area allowed to obtain reliable PS points just on the south-eastern faces of towers 1, 2, and 3 (Fig. 4a). However, PS points
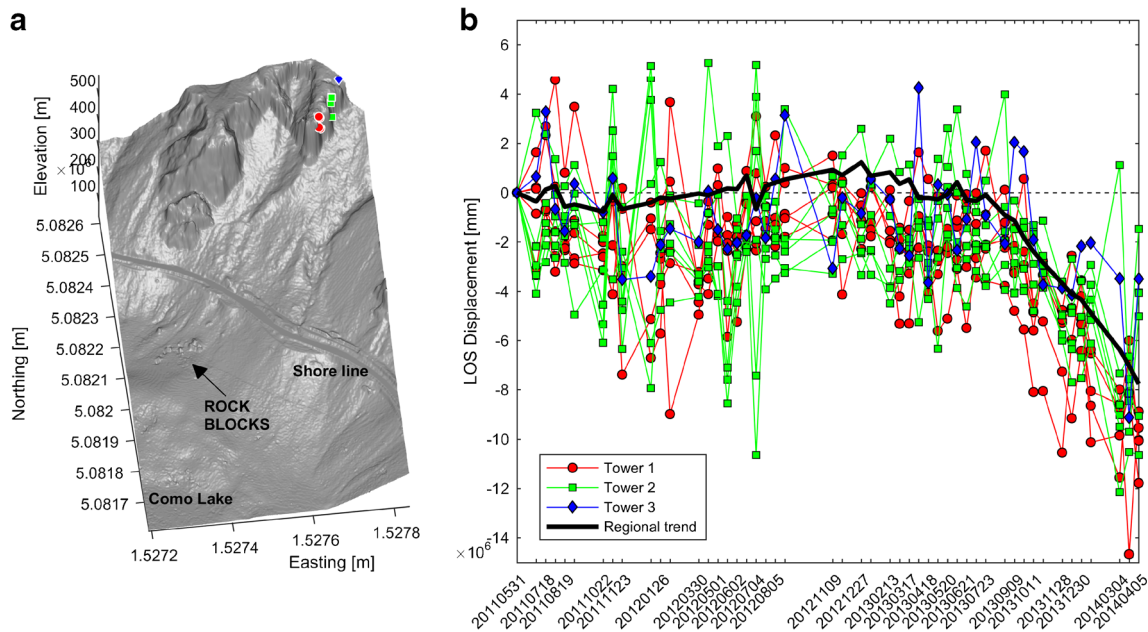
**Fig. 4** **a** The 2 × 2-m DTM of the investigated area with bathymetry; persistent scatterers identified with the COSMO-SkyMed satellites are also displayed on towers 1, 2, and 3. **b** Line-of-sight displacements obtained from the persistent scatterer dataset (descending satellite orbit only)

were retrieved only for the descending satellite orbits so it was not possible to decompose the estimated line-of-sight (LOS) PS displacements into their horizontal and vertical components. The plot of the LOS displacements versus time reveals that, after approximately 2.5 years without any noticeable trend, PS points started to move consistently in late summer 2013. Considering that the LOS unit vector is (− 0.085993, 0.439155, 0.894286), respectively, for the north, east, and vertical components, the towers seem to be mainly affected by downward movements with a small component to the west. Anyway, the analysis of an area of approximately 2.5 km² centred on the rock towers and grouping about 2000 PS points (both natural and human-made reflectors) reveals a similar average displacement trend (Fig. 4b). This result suggests that the movements identified on the towers may be related to regional trends due to either processing artefacts or a bad reference point used to compute PS relative displacements. We deem a general sinking of the investigated area to be unlikely and so, this provides no useful information about the stability conditions of *Torrioni di Rialba*.

### Geophysical investigations

Geophysical methodologies have been used extensively to characterise unstable slopes in a non-destructive manner (Bichler et al. 2004; Roch et al. 2006; Lundström et al. 2009; Bièvre et al. 2016; Palis et al. 2017; Stucchi et al. 2017). Amongst the geophysical techniques that could be used to effectively study the shale layer in the slope under investigation, seismic methods were considered because of the contrast in seismic (P wave) velocities between *San Giovanni Bianco* formation and other rock formations discussed earlier (Table 2). Considering that a very important goal would be detecting the shale layer just below the rock towers, a seismic traveltime tomography experiment was a reasonable approach. However, because of the possible limited thickness of the low-

velocity shale layer embedded within the *Rialba* conglomerate and *Gorno* limestone (Table 2), P wave first arrivals are most likely to give information about higher-velocity formations. In addition, the harsh terrain with rough topography and thick vegetation poses considerable constraints for deploying seismic sources and cables to obtain an accurate tomographic image of the subsurface. To this end, we performed a series of transillumination seismic tests (a class of seismic tomography with a limited number of channels) around tower 1 with portable lightweight equipment, placing six source points and seven geophones on the western/south-western side and on the eastern side, respectively. Initial tests performed with a source-sensor couple placed directly on the conglomerate at the base of tower 1 yielded a mean velocity of 2050 m/s, that is, 30 to 50% lower than the values listed in Table 2. This is attributed to the effect of fractures, lower cementation at the base of the tower and lower frequencies of the seismic waves involved with respect to the laboratory tests. Computation of velocities assuming linear travel paths gave values between 1100 and 1500 m/s, with a consistent decreasing trend associated to the different source points, travelling from west to south-west, that is thought to be caused by increasing thickness of surface debris layer.

### Geoelectrical surveys

Electrical methods are very well suited to detect the presence of a conductive shale layer within resistive formations such as the *Rialba* conglomerate and *Gorno* limestone. More in details, electrical resistivity tomography (ERT) is an imaging technique now widely applied to the investigation of landslides in various lithological contexts (from fine-grained soils to compact and cemented rocks). Fundamentals about the technique can be found in reference books (e.g. Reynolds 2011) and specifics about landslide

investigation are exposed in more or less recent review articles (Jongmans and Garambois 2007; Perrone et al. 2014).

We ran four ERT profiles at different elevations and with various orientations along the slope. The profiles conducted in this work are labelled E1 to E4 and their location is shown in Fig. 3a. Measurements were collected with a SYSCAL-Pro resistivimeter working with 48 electrodes and the spread had a constant electrode spacing of 1 m (E1 and E2), 2 m (E3) and 3 m (E4), respectively. Profile E2 was the only one collected according to the roll-along mode, with a single shift of 24 electrodes. Electrodes were georeferenced in the field using GNNS receivers, and accurate elevations were further extracted from a digital elevation model (DEM) with a grid size of 2 m. To achieve both good vertical and lateral resolution along with a high signal-to-noise (SNR) ratio, measurements were carried out using both the Wenner and Schlumberger configurations. For the former configuration, the spacing between the electrodes was varied between 1 and 15 single-electrode spacing, whilst for the latter, the spacing between potential electrodes was kept to 1 electrode spacing, and the spacing between current electrodes varied between 1 and 15. Experimental data were filtered by removing strong outliers and also measurements with very low potential values. Table 3 reports the characteristics of the surveys as well their inversions.

Experimental data were inverted using the Boundless Electrical Resistivity Tomography (BERT) software package developed by Günther et al. (2006) that uses finite element computations with irregularly shaped triangles (Rücker et al. 2006). For profiles E1 to E3, resistance values were used to force the algorithm to compute ad hoc 2D geometric factors. Considering that profile E4 is not entirely linear (Fig. 3a), we decided to compute the 3D geometric factor of each measurement using the methodology proposed by Bièvre et al. (2018). Accordingly, we used the measured resistance values and the geometric factors computed a posteriori to correct the apparent resistivity data for 3D topographic effects and we obtained variations in inverted resistivities up to 30% and down to − 20% with respect to the 2D approach.

As far as the inversion procedure is concerned, we set homogenous starting models with resistivity equal to the mean apparent resistivity of each pseudo-section. The investigation depth was computed automatically. In the iterative process, we used the L1 norm to enhance the contrasts between adjacent lithological units. The discrepancy between experimental and theoretical data was evaluated with a chi$^2$ test (Günther et al. 2006). This test normalises the residuals by a measurement error of several percent (voltage error and geometrical error). For the four profiles, chi$^2$ values close to 1 were obtained after a few iterations by manually tuning the regularisation strength, indicating that the data were

fitted within an error of 3% (default value). All relative root mean square (RRMS) errors were below 10% (Table 3).

Inverted resistivity sections are presented in Fig. 5 with a common colour scale ranging from 25 to 2500 Ωm. The degree of transparency on the images corresponds to the sensitivity matrix: the higher the transparency is, the lower the sensitivity is. In all sections it is generally possible to identify two main units: one with resistivity from 25 to around 100 Ωm and a second with resistivity ranging between 100 and 2500 Ωm. The low-resistivity unit could be associated with the shale layer, because spread E1 was partly deployed on the outcrop of *San Giovanni Bianco* formation found close to the springs adjacent to the base of the glacial terrace (Fig. 3a, c). We deem that high resistivity values may be associated with *Rialba* conglomerate and slope debris coming mainly from the *Rialba* Towers and partly from the neighbouring *Esino* limestone rock cliffs. One may speculate that an additional unit with resistivity between 200 and 400 Ωm (greenish colour in Fig. 5) is placed between the (shallower) high and (deeper) low-resistivity formations. This unit could be associated with *Rialba* conglomerate more compact than the surface one or with conglomerate that was partially mixed with the underlying shale during the sliding process described above.

Organic soil was found at a few places along spreads E2 and E3 where lower resistivity values are observed at the surface. It is interesting to note that shallow higher resistivity values at the beginning of profile E3 (Fig. 5c) correspond to an outcrop of *Rialba* conglomerate (Fig. 2b) that we mapped on site. In addition, the sharp resistivity variation at about 35 m along profile E4 (Fig. 5d) may be due to the continuation of the fault between *Rialba* conglomerate and *Esino* limestone formations that can be observed upslope (Fig. 2b). No evidence of shale was found at the end of spread E4, so that very low resistivity values at the surface may be due to wet organic soil (Fig. 5d).

### Seismic noise surveys

Since previous monitoring activities involving quasi-static measurements of displacement by means of extensometers, prism reflectors and persistent scatterer interferometry gave no significant results, we deemed it useful to perform dynamic measurements with seismic sensors and exploit ambient vibrations to investigate the vibration modes of the towers and, possibly, their change with time associated to the variations of the stability conditions (Bottelin et al. 2017; Kleinbrod et al. 2017; Taruselli et al. 2019).

With respect to classical microseismic monitoring of unstable slopes (e.g. Arosio et al. 2018), seismic noise recordings can be collected continuously without the need for any specific seismic

**Table 3** Characteristics of ERT acquisitions and of the inversion results

| Profile | Electrodes Number | Spacing (m) | Number of data | Iterations | Chi$^2$ | RRMS (%) |
|---------|-------------------|-------------|----------------|------------|---------|----------|
| E1 | 48 | 1 | 840 | 5 | 0.65 | 6.6 |
| E2 | 72 | 1 | 1440 | 6 | 0.97 | 6.6 |
| E3 | 48 | 2 | 840 | 4 | 0.8 | 8 |
| E4 | 48 | 3 | 619 | 5 | 0.98 | 7 |

RRMS relative root mean square error
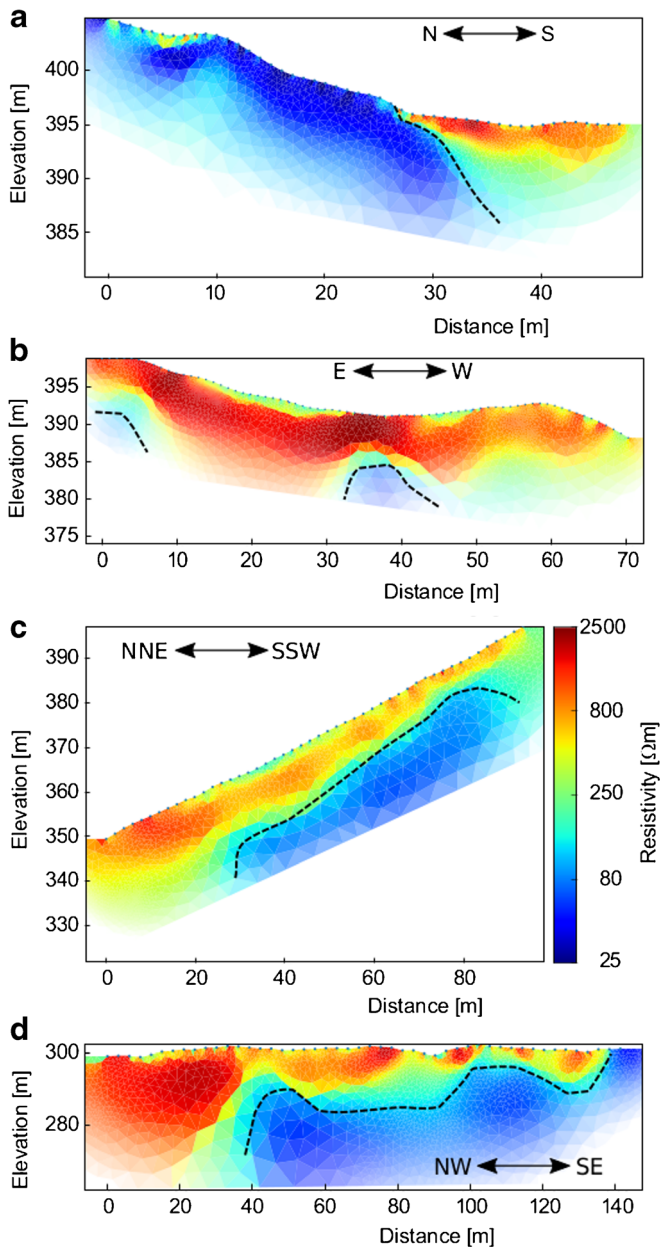
**Fig. 5** Electrical resistivity tomography results for profiles **a** E1, **b** E2, **c** E3 and **d** E4. The resistivity sections are represented with a common colour scale. The blacks dashed lines correspond to isocontours of 90 Ωm

event generated by collapses or fracture propagation. A very common approach to monitor rock cliffs is to deploy three-component seismic sensors and compute the horizontal-to-vertical spectral ratio (HVSR), after time series are transformed into their amplitude spectra. Robust peaks in the HVSR plot indicate the presence of preferential vibration modes of the monitored structure with sufficient energy. The three-component recordings are first bandpass filtered to discard both low-frequency trends and high-frequency noise. Then they are divided into smaller windows, generally applying window overlapping and tapering. Non-stationary time windows are rejected and amplitude spectra are computed for each window, with some degree of frequency-dependent smoothing (e.g. Konno and Ohmachi 1998). The north and east components are merged into the horizontal component and the HVSR is computed. Finally, all the HVSRs are averaged using a quadratic mean that is most sensitive to low values so as to produce a robust HVSR estimate.

We performed two seismic noise field campaigns in January 2017 and March 2018. During the first measurement session, we deployed 20-s Nanometrics Trillium 3C geophones at the top of each tower plus one on the top stable rock mass to be used as a reference (Fig. 3a). In the second session, we surveyed the previous points and, in addition, we also deployed four sensors at the base of the towers, two on the western side and two on the eastern one (Fig. 3a) to investigate possible amplification phenomena of the ambient vibration wave-field soliciting the rock towers.

The datasets collected indicate that the amplitude of the vertical component is regularly smaller with respect to the amplitude of the horizontal components, excluding data recorded on tower 4 and at the base of the eastern side of the towers (Fig. 6). Ambient vibrations at the same locations across the two monitoring sessions do not appear to have constant features, apart from data collected on tower 1, whose horizontal amplitude is steadily much higher than the vertical component. In general, we can observe a slight-to-moderate amplification of signals recorded on the towers with respect to the signals recorded on the stable rock mass and at the base of the towers (Fig. 6). Plots of the HVSRs obtained at each location offer a clearer picture as they indicate that results are stable in the two monitoring sessions and that strong peaks are only discernible for towers 1 and 2 (Fig. 7). In more detail, tower 2 displays a sharp high-amplitude peak at about 1.90 Hz, with the remaining HVSR curve close to 1 and with low standard deviation. On the contrary, tower 1 seems to show a complex behaviour, especially in the 0.02–1.50-Hz frequency range where high HVSR values and large standard deviation could possibly be related to several overimposed vibration modes due to the complex geometry of the tower, including the erosion cave in the lower part (Fig. 3h) and the complex trend of the fracture F1 on the north-western side (Fig. 2). The other locations measured do not show any significant HVSR peaks, at least at frequencies that could be usually associated to vibration mode of the investigated structures, and feature low standard deviations. The analysis of the HVSRs as a function of azimuth (Fig. 8a) reveals that tower 2 seems to display two different, though close, resonance frequencies: the one with highest energy at about 1.93 Hz along the 45°–225° direction and a lower energy one at 1.80 Hz and oscillation along the 125°–305° direction. Tower 1 has again a more complex situation with low-frequency spectral features changing across the two measurements, but a constant peak at about 1.90 Hz along the 15°–195° direction that can be identified also in the HVSR plots (Fig. 8a). When computing the HVSRs as a function of azimuth, it is important to note that spectral smoothing should be applied carefully because it may merge vibration modes with different directions but similar frequencies.

By comparing the plots in Fig. 8a with the datasets collected at meteorological station about 1.8 km from the site, we suggest that the oscillation in the direction 125°–305° may be caused by the wind. Actually wind was present in both measurement sessions (Fig. 8b) and during the day with the strongest wind (i.e. 26 January 2017) we observed a higher amplitude peak of the
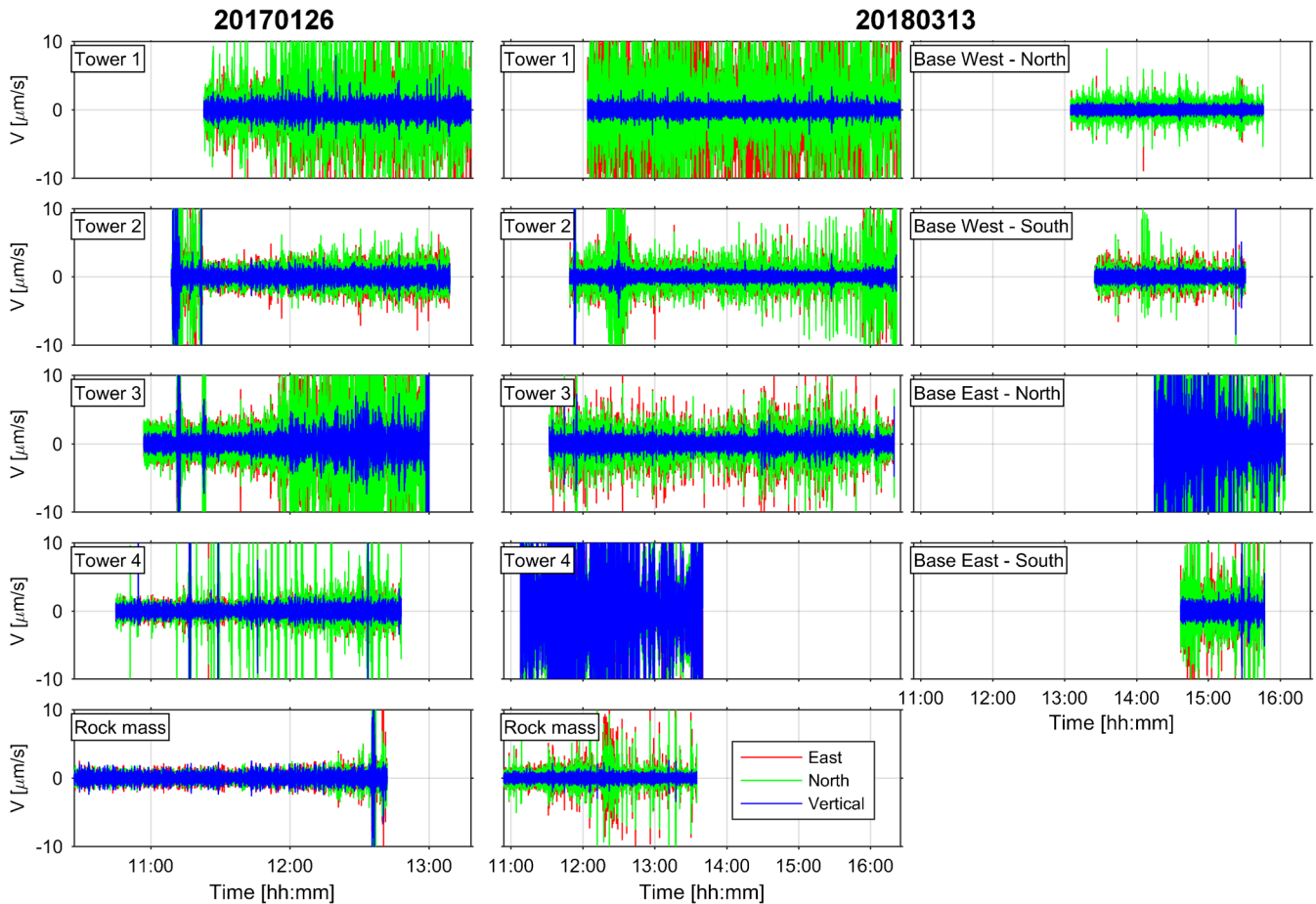
**Fig. 6** Seismic noise signals collected in the two recording sessions

vibration mode. Temperature may also affect the vibration mode of the rock structures, although previous studies (e.g. Colombero et al. 2017) seem to suggest that the temperature difference across the two measurements (Fig. 8c) is not enough to generate an appreciable variation of the frequencies.

### Discussion and conclusions
Complex geological scenarios require information retrieved by means of diverse investigation techniques to be merged in order to provide a comprehensive understanding and to identify ongoing processes involved (Merritt et al. 2014; Mulas et al. 2018). Because of the complex geological history of the investigated site, mainly related to past tectonic events, in this work we resort to the integration of geological, geomechanical and geophysical surveys to define as accurately as possible a physical model of the slope.

From a geomechanical perspective, it is reasonable to assume a shale layer below all the conglomerate towers since the four major fractures separating the rock pillars (Fig. 2) could have been generated by separation of the rigid conglomerate rock body overlying softer plastic shale layer (Price 2009). This layer likely extends below the glacial terrace, as suggested by the shale outcrops on its north-western side and by the fact that major fractures seem to affect both the rock towers and the glacial terrace itself

(Fig. 2c). In addition, springs immediately next to fracture F2 further support the presence of an impermeable argillaceous rock layer at the base of the cliff.

After field surveys were completed, we focused attention on the characterisation of the *San Giovanni Bianco* formation in terms of attitude and depth of the plastic layer. In particular, the ERT sections identified low-resistivity areas associated with the *San Giovanni Bianco* shale. Considering the resistivity values observed in the sections, the values commonly found in the scientific literature for shale rocks (e.g. Lowrie 2007; Reynolds 2011), and the field calibration obtained with the electrodes of spread E1 (Figs. 3a and 5a) directly deployed into the shale (though wet), it is reasonable to assign a range from 25 to 90 $\Omega$m. We then computed the plane that best fits points belonging to the top of the shale layers in each section as the least square of the distance to the plane. The computed plane is approximately 10 m below the surface, parallel to the slope (attitude 205°/31°), and outcrops close to spread E1 and to the springs (Fig. 9a) where shale outcrops were observed (Fig._ 3c). That the *San Giovanni Bianco* layer seems to lie parallel to the slope supports the hypothesis of a collapse in late Miocene times that failed over the shale layer and that later lithified into the *Rialba* conglomerate. The resistivity section of spread E1 together with the interpretation of the boreholes also suggests that the *San*
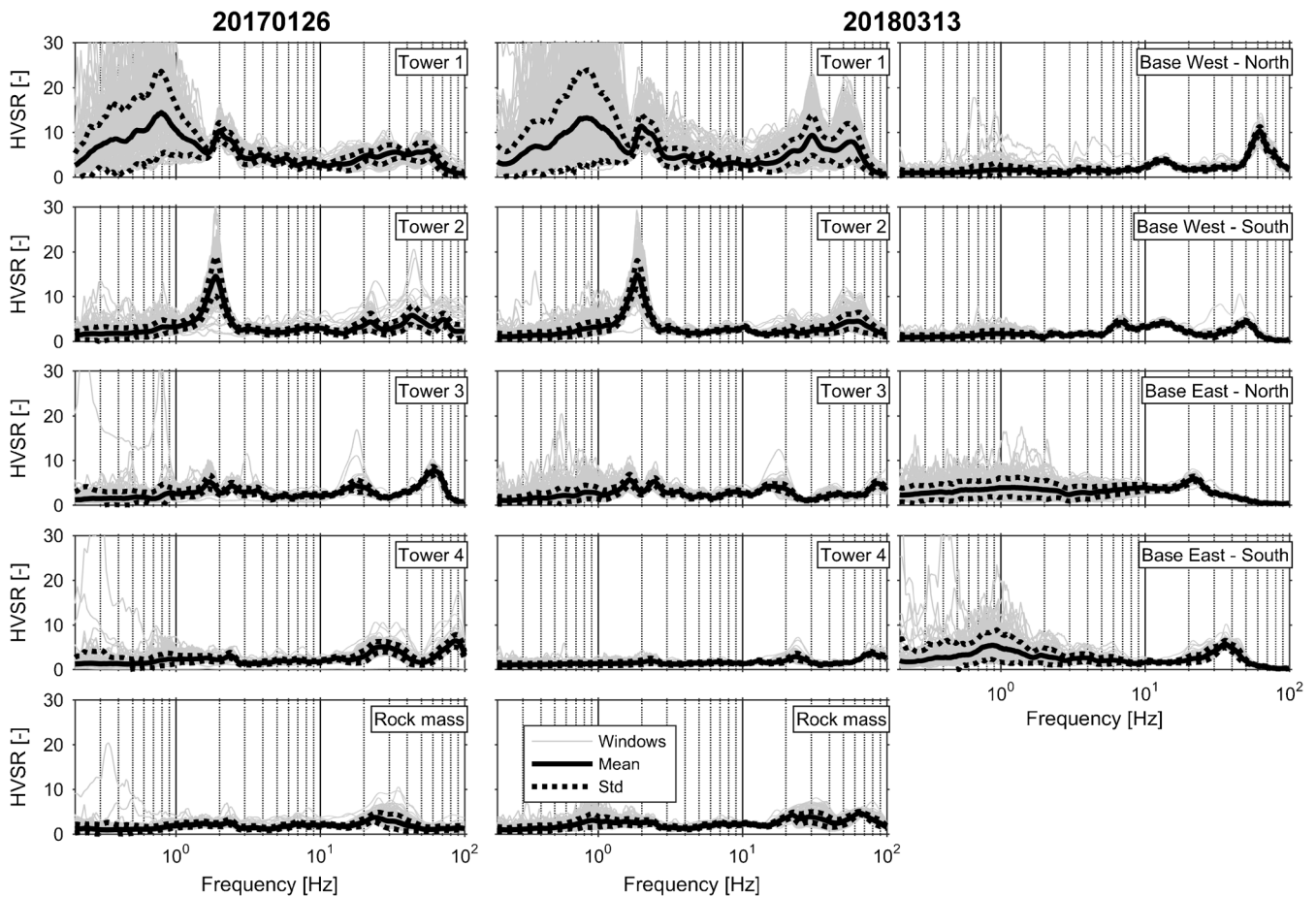
**Fig. 7** HVSR estimates obtained from the seismic noise collected in the two recording sessions

*Giovanni Bianco* layer could be very thin (i.e. around 20–25 m), although the investigation depth of the ERT surveys prevents any accurate assessment.

The combination of different survey techniques leads to a geological model of the *Rialba towers* depicted in Fig. 10. Regarding kinematic analysis, the plastic shale layer underneath the rock cliff is very likely to promote a lateral spreading phenomenon, involving slow displacements, but that can also evolve into faster movements. The presence of a rock spur downslope of tower 1 (Figs. 2, 9b, and 10) together with the large rock blocks found in the bathymetric survey (Fig. 4a) suggest that an additional rock pillar may have toppled and fallen into the lake. Although a conventional back-analysis of the collapse cannot be performed (e.g. Spreafico et al. 2016), it may be assumed that failure was favoured by the weak subhorizontal layer of weakly cemented conglomerate that matches the eroded cavity in the lower section of tower 1 (Figs. 2c, d and 3h). Unfortunately, there is no information about the extent of the weak layer within the cliff, so that it is not possible to determine whether this layer could affect the stability of one or more towers (Fig. 10b). As far as we are aware, we deem that the most probable failure mechanism would be the toppling of tower 1, promoted primarily by the weak conglomerate layer. After the failure is triggered, the evolution of the kinematic behaviour into sliding, falling, etc.,

related to further breakdown of the rock tower, is hard to judge at present. The minor discontinuity sets affecting the cliff and large blocks found in the lake suggest that failing rock blocks may have considerable size. Consequently, any risk management strategy should take into account the effects and impacts of a possible tsunami.

In addition, weathering associated with groundwater circulation can contribute to instability of the towers because of (i) widening and deepening of the major fractures, karst phenomena and erosion, especially if located at the base of the towers; (ii) freeze-thaw cycles causing normal stresses within the fractures; and (iii) stresses due to clay-swelling related mechanisms affecting the shale layer.

A kinematic analysis of the unstable slope can support the evaluation of possible risk scenarios and help in the design of mitigation structures and effective monitoring strategies using both standard and novel techniques. Monitoring activities performed so far involving both close- and long-range remote sensing measurements have not detected appreciable permanent displacements, although it is still not clear if there were actually no displacements, or whether the displacement rate was not significant during the monitoring period. In this respect, seismic noise spectral analysis is an emerging geophysical methodology that provides information about subtle changes in the
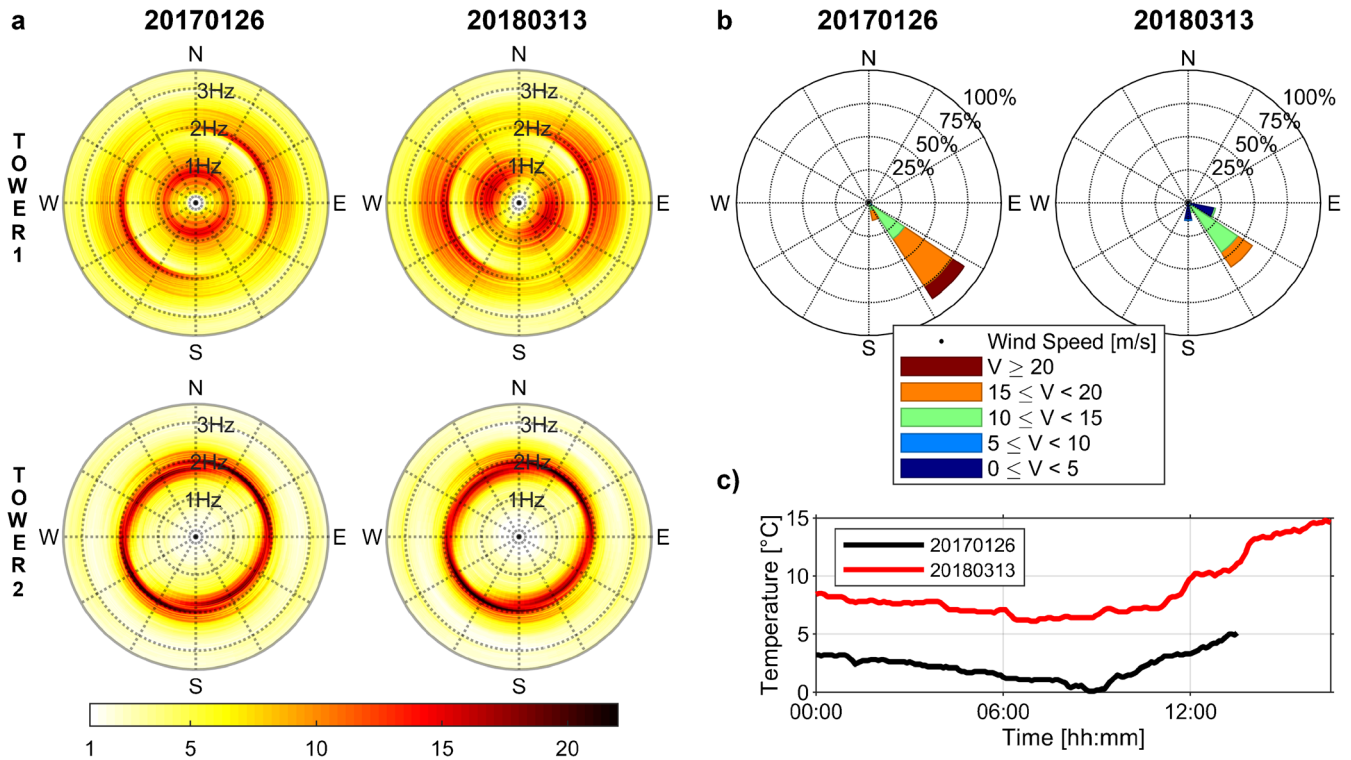
Fig. 8 **a** HVSRs computed as a function of azimuth. **b** Wind rose plot and **c** temperatures collected during the two recording sessions

stability conditions of rock structures not necessarily associated with permanent displacements. The seismic noise measurements carried out in this study suggest that no significant variations across the two sessions, especially considering the

spectral features of towers 1 and 2, show high values in their HVSRs. In our geological model, a hypothetical shale layer lies below all the towers. The difference in the HVSR values can be attributed to the fact that towers 1 and 2 are well separated from
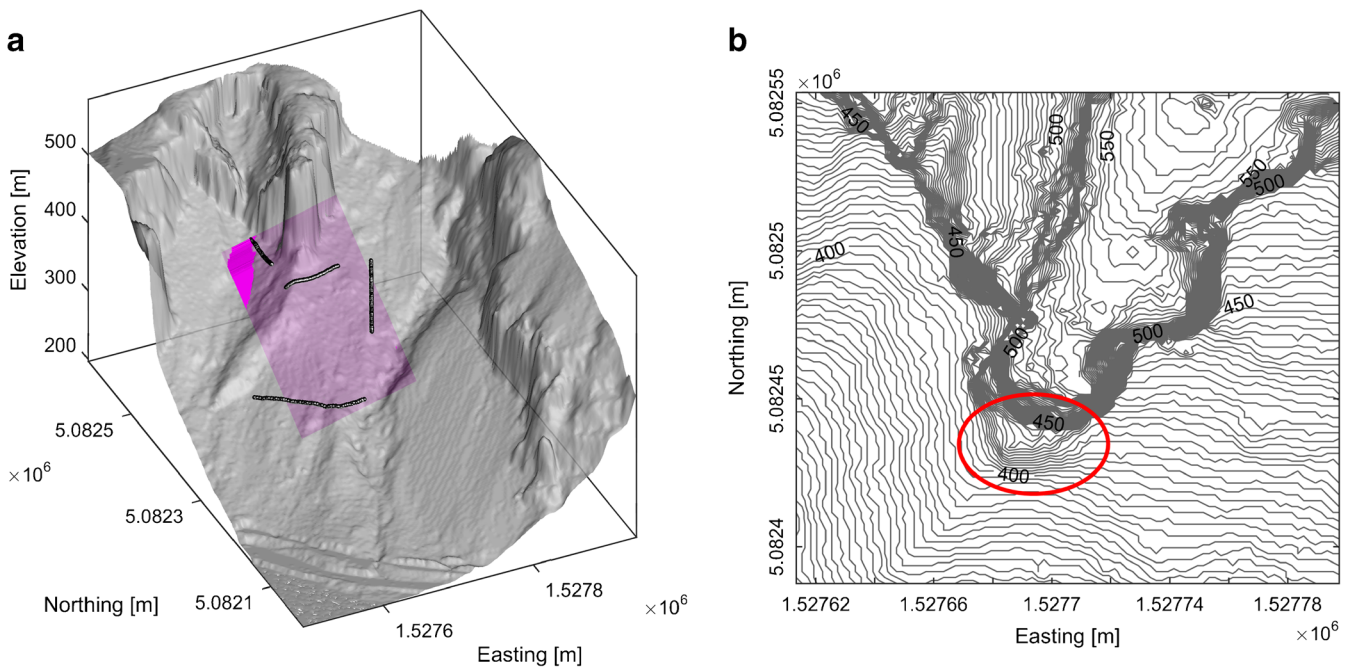


Fig. 9 **a** The 2 × 2-m DTM of the investigated area with the best fit plane (magenta surface) representing the top of the shale layer obtained by interpreting the results of the ERT surveys (black lines). **b** Isolevel contours with a close up of towers 1 and 2; red ellipse borders the area with the remains of a supposed former additional rock pillar
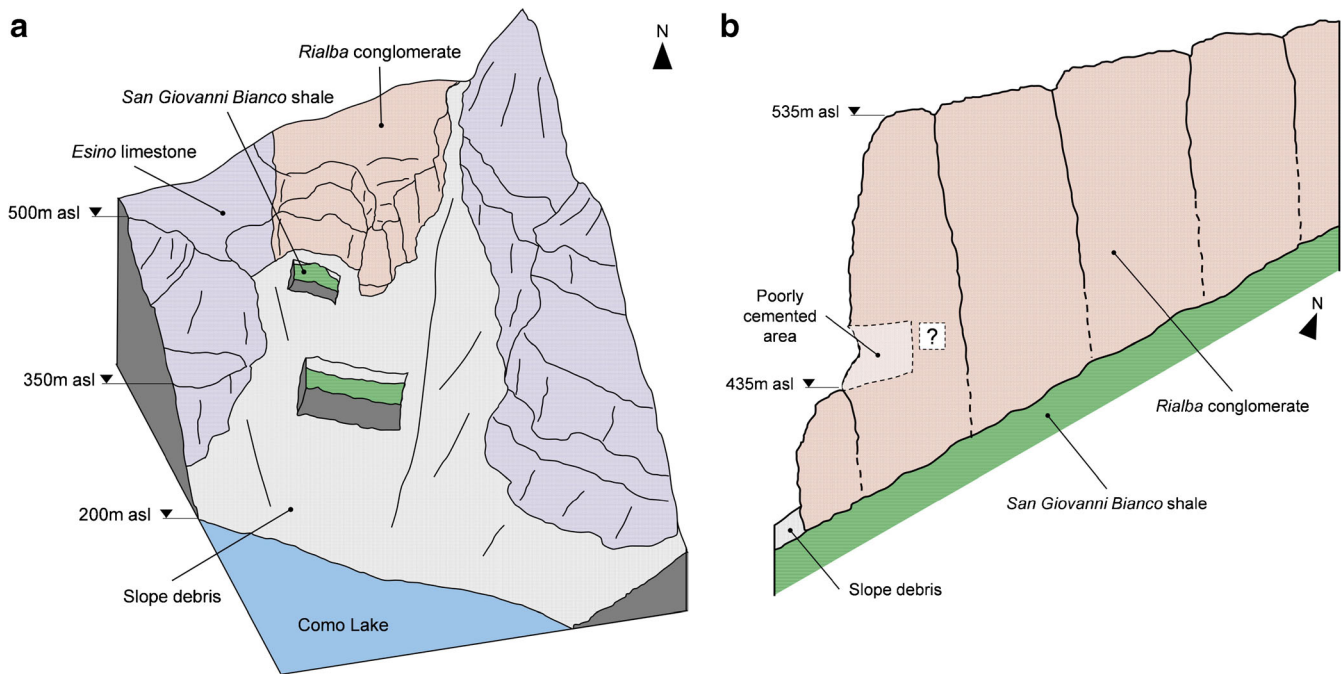
**Fig. 10** **a** 3D geological sketch of the *Torrioni di Rialba* area and **b** cross-section sketch of the rock towers according to the results of our investigations. The question mark indicates that there is no information about the extent of the poorly cemented area within the cliff

the rock cliff, with fractures F1 and F2 containing very large apertures and persistence. HVSR as a function of azimuth proves to be very useful in understanding preferential vibration directions with respect to the HVSR alone.

To obtain indications about the order of magnitude of the theoretical vibration frequencies of the rock towers, we can consider the natural vibration frequency of a cantilever beam with uniform mass per unit length $m$ (kg/m). Taking into account only the deflection associated with bending stress in the beam and neglecting the effect of rotational inertia and shear deformation, the $n$th resonance frequency can be expressed as (Chopra 2012)

$$f_n = \frac{K_n}{2\pi} \sqrt{\frac{EI}{mH^4}}$$

where $E$ is the Young's modulus (Pa), $I$ is the area moment of inertia (m⁴), $H$ is the length of the beam (m) and $K_n$ is a dimensionless coefficient that varies according to the vibration mode (e.g. 3.516 for the first mode). For each tower, we computed the mean value and the standard deviation of the first four vibration mode frequencies (Table 4) by considering an accuracy of ± 5% in the geometrical parameters reported in Table 1; the range of $E$ reported in Table 2 for *Rialba* conglomerate, with its density spanning from 2500 to 3000 kg/m³; and the area moment of inertia was computed by considering two orthogonal rotation axes parallel to the sides of the (approximated) rectangular base of each tower.

Although the resonance frequencies obtained are to be considered estimates, they provide indications of the expected

values. In particular, it is interesting to note that the first vibration mode for tower 2, when considering the barycentric axis parallel to the longer side of the rectangular base ($L$), has a frequency very close to that estimated with the HVSR method. In addition, this vibration direction is in accordance with the one associated with the lower resonance frequency identified in the plot of the HVSR as a function of azimuth (Fig. 8a). Moreover, the frequency computed for the first vibration mode of tower 1 (Table 4) appears to be close to the results provided by the HVSR analysis, although a comparison between the analytical and experimental vibration directions is more difficult to make in this case.

Seismic noise tests have provided preliminary outcomes, since a rigorous investigation should involve continuous monitoring for an extended time length and through different climatic conditions, especially where unstable slopes lack clear indications of collapse. With respect to this, the results provided by analysis of the HVSR as a function of azimuth may also help to design suitable monitoring strategies by considering the direction of preferential displacement of the towers, i.e. the direction along which displacements are expected to be greater. For instance, a ground-based interferometric microwave radar could be coupled to continuous monitoring with seismic noise sensors since they have the capability to monitor displacements in terms of accuracy and frequency. Satellite-based interferometry is also suited for monitoring slow movements related to lateral spreading phenomena. This technique could be performed on more recent PS datasets, although this would only measure those subvertical displacements of the rock mass whose movements are driven by the lateral spreading of the underlying weak shale layer.

**Table 4** First four vibration mode frequencies of the rock towers considering area moments of inertia for the barycentric axis parallel (left) and perpendicular (right) to the longer side of the rectangular base, respectively

| Tower | Vibration mode frequency (Hz) ($I = LW^3/12$) | | | | Vibration mode frequency (Hz) ($I = WL^3/12$) | | | |
|---|---|---|---|---|---|---|---|---|
| | First mode | Second mode | Third mode | Fourth mode | First mode | Second mode | Third mode | Fourth mode |
| T1 | *1.1 ± 0.3* | 7.1 ± 1.7 | 19.8 ± 4.9 | 38.9 ± 9.6 | 2.4 ± 0.4 | 15.0 ± 2.3 | 42.1 ± 6.4 | 82.4 ± 12.6 |
| T2 | *2.1 ± 0.5* | 13.3 ± 3.3 | 37.2 ± 9.2 | 72.9 ± 18.0 | 5.1 ± 0.8 | 32.3 ± 4.9 | 90.4 ± 13.8 | 177.0 ± 27.0 |
| T3 | 2.5 ± 0.6 | 15.9 ± 3.9 | 44.7 ± 11.0 | 87.6 ± 21.6 | 7.3 ± 1.1 | 45.6 ± 7.0 | 127.7 ± 19.5 | 250.3 ± 38.2 |
| T4 | 4.0 ± 1.0 | 25.1 ± 6.2 | 70.4 ± 17.3 | 138.0 ± 34.0 | 11.8 ± 1.8 | 74.0 ± 11.3 | 207.4 ± 31.7 | 406.4 ± 62.0 |

Mean values are reported with plus/minus the standard deviations. $I$ is the area moment of inertia and $L$ and $W$ are the longer and shorter sides of the rectangular base of the towers, respectively. See text for details

Values in italic closely match the resonance frequencies obtained by processing seismic noise data

## References

Arosio D, Longoni L, Papini M, Boccolari M, Zanzi L (2018) Analysis of microseismic signals collected on an unstable rock face in the Italian Prealps. Geophys J Int 213:475–488

Aydin A, Basu A (2005) The Schmidt hammer in rock material characterization. Eng Geol 81:1–14

Bichler A, Bobrowsky P, Best M, Douma M, Hunter J, Calvert T, Burns R (2004) Three-dimensional mapping of a landslide using a multi-geophysical approach: the Quesnel Forks landslide. Landslides 1:29–40

Bièvre G, Jongmans D, Goutaland D, Pathier E, Zumbo V (2016) Geophysical characterization of the lithological control on the kinematic pattern in a large clayey landslide (Avignonet, French Alps). Landslides 13:423–436

Bièvre G, Oxarango L, Günther T, Goutaland G, Massardi M (2018) Improvement of 2D ERT measurements conducted along a small earth-filled dyke using 3D topographic data and 3D computation of geometric factors. J Appl Geophys 153:100–112

Bini A, Zuccoli L, Bussolini C, Corbari D, Da Rold O, Ferliga C, Rossi S, Viviani C (2004) Glacial history of the southern side of the Central Alps, Italy. Dev Quat Sci 2:195–200

Booth AM, Dehls J, Eiken T, Fischer L, Hermanns RL, Oppikofer T (2015) Integrating diverse geologic and geodetic observations to determine failure mechanisms and deformation rates across a large bedrock landslide complex: the Osmundneset landslide, Sogn og Fjordane, Norway. Landslides 12:745–756

Bottelin P, Baillet L, Larose E, Jongmans D, Hantz D, Brenguier O, Cadet H, Helmstetter A (2017) Monitoring rock reinforcement works with ambient vibrations: La Bourne case study (Vercors, France). Eng Geol 226:136–145

Carobene L, Cevasco A (2011) A large scale lateral spreading, its genesis and quaternary evolution in the coastal sector between Cogoleto and Varazze (Liguria-Italy). Geomorphology 129(3–4):398–411

Chelli A, Mandrone G, Truffelli G (2006) Field investigations and monitoring as tools for modelling the Rossena castle landslide (northern Appennines, Italy). Landslides 3:252–259

Chopra AK (2012) Dynamic of structures. Theory and applications to earthquake engineering, 4th edn. Prentice Hall

Colombero C, Baillet L, Comina C, Jongmans D, Vinciguerra S (2017) Characterization of the 3-D fracture setting of an unstable rock mass: from surface and seismic investigations to numerical modelling. J Geophys Res Solid Earth 122:6346–6366

Costantini M, Falco S, Malvarosa F, Minati F (2009) Trillo F (2009) Method of persistent scatterer pairs (PSP) and high resolution SAR interferometry. IEEE Int Geosci Remote Sens Symp 3:904–907

Gianotti R, Perotti CR (1986) Introduzione alla tettonica e all'evoluzione strutturale delle Alpi Lariane. Mem Soc Geol Ital 32:67–99

Günther T, Rücker C, Spitzer K (2006) Three-dimensional modelling and inversion of DC resistivity data incorporating topography—II. Inversion. Geophys J Int 166:506–517

Hungr O, Leroueil S, Picarelli L (2014) The Varnes classification of landslide types, an update. Landslides 11:167–194

IFFI, Inventario dei Fenomeni Franosi in Italia, (2018). http://www.progettoiffi.isprambiente.it/cartanetiffi/, last accessed on 25/09/2018

Jongmans D, Garambois S (2007) Geophysical investigation of landslides: a review. Bulletin de la Société Géologique de France 178:101–112

Katz O, Reches Z, Roegiers JC (2000) Evaluation of mechanical rock properties using a Schmidt hammer. Int J Rock Mech Min Sci 37:723–728

Kleinbrod U, Burjánek J, Fäh D (2017) On the seismic response of instable rock slopes based on ambient vibration recordings. Earth Planets Space 69:126

Konno K, Ohmachi T (1998) Ground-motion characteristic estimated from spectral ratio between horizontal and vertical components of microtremor. Bull Seismol Soc Am 88:228–241

Laubscher HP (1985) Large-scale, thin-skinned thrusting in the southern Alps: kinematic models. Geol Soc Am Bull 96:710–718

Lowrie W (2007) Fundamentals of geophysics, 2nd Edition. Cambridge University Press

Lundström K, Larsson R, Dahlin T (2009) Mapping of quick clay formations using geotechnical and geophysical methods. Landslides 6:1–15

Merritt AJ, Chambers JE, Murphy W, Wilkinson PB, West LJ, Gunn DA, Meldrum PI, Kirkham M, Dixon N (2014) 3D ground model development for an active landslide in Lias mudrocks using geophysical, remote sensing and geotechnical methods. Landslides 11:537–550

Mulas M, Ciccarese G, Ronchetti F, Truffelli G, Corsini A (2018) Slope dynamics and streambed uplift during the Pergalla landslide reactivation in March 2016 and discussion of concurrent causes (northern Apennines, Italy). Landslides 15:1881–1887

Palis E, Lebourg T, Vidal M, Levy C, Tric E, Hernandez M (2017) Multiyear time-lapse ERT to study short- and long-term landslide hydrological dynamics. Landslides 14:1333–1343

Pasuto A, Soldati M (1996) Rock spreading. In: Dikau R, Brunsden D, Schrott L, Ibsen ML (eds) Landslide recognition: identification, movement and causes. John Wiley & Sons, Chichester, UK, pp 122–136

Pasuto A, Soldati M (2013) Lateral spreading. In: Shroder J (ed) Treatise on geomorphology, Elsevier, pp. 239–248

Perrone A, Lapenna V, Piscitelli S (2014) Electrical resistivity tomography technique for landslide investigation: a review. Earth Sci Rev 135:65–82

Picarelli L, Russo C (2004) Mechanics of slow active landslides and interaction with manmade works. In: Lacerda WA, Ehrlich M, Fontoura SAB, Sayao ASF (eds) Landslides. Evaluation & Stabilization, A.A. Balkema, Rotterdam, pp 1141–1176

Price DG (2009) Engineering geology—principles and practice. Springer

Reynolds JM (2011) An introduction to applied and environmental geophysics, 2nd Edition. Wiley-Blackwell

Roch KH, Chwatal W, Brückl E (2006) Potentials of monitoring rock fall hazards by GPR: considering as example the results of Salzburg. Landslides 3:87–94

Rücker C, Günther T, Spitzer K (2006) Three-dimensional modelling and inversion of DC resistivity data incorporating topography—I. Modelling. Geophys J Int 166:495–505

Sharma PK, Khandelwal M, Singh TN (2011) A correlation between Schmidt hammer rebound numbers with impact strength index, slake durability index and $P$-wave velocity. Int J Earth Sci 100:189–195

Soldati M (2013) Deep-seated gravitational slope deformation. In: Bobrowsky PT (ed) Encyclopedia of natural hazards. Springer, Dordrecht, pp 151–155

Soldati M, Pasuto A (1991) Some cases of deep seated gravitational deformations in the area of Cortina d'Ampezzo (Dolomites): implications in environmental risk assessment. In: Panizza M, Soldati M, Coltellacci MM (eds) Proceedings of the European Experimental Course on Applied Geomorphology. Istituto di Geologia, Università degli Studi di Modena, Modena, pp 91–104

Spreafico MC, Cervi F, Francioni M, Stead D, Borgatti L (2017) An investigation into the development of toppling at the edge of fractured rock plateaux using a numerical modelling approach. Geomorphology 288:83–98

Spreafico MC, Francioni M, Cervi F, Stead D, Bitelli G, Ghirotti M, Girelli VA, Lucente CC, Tini MA, Borgatti L (2016) Back analysis of the 2014 San Leo landslide using combined terrestrial laser scanning and 3D distinct element modelling. Rock Mech Rock Eng 49:2235–2251

Stucchi E, Tognarelli A, Ribolini A (2017) SH-wave seismic reflection at a landslide (Patigno, NW Italy) integrated with $P$-wave. J Appl Geophys 146:188–197

Taruselli M, Arosio D, Longoni L, Papini M, Corsini A, Zanzi L (2019) Rock stability as detected by seismic noise recordings—three case studies. Proceedings of the 24th European Meeting of Environmental and Engineering Geophysics, Portugal, pp 9–13 September 2018; Code 143674

Viero A, Teza G, Massironi M, Jaboyedoff M, Galgaro A (2010) Laser scanning-based recognition of rotational movements on a deep seated gravitational instability: the Cinque Torri case (north-eastern Italian Alps). Geomorphology 122:191–204

**D. Arosio** (✉)
Department of Chemical and Geological Sciences,
Università degli Studi di Modena e Reggio Emilia,
Via Giuseppe Campi 103, 41125, Modena, Italy
Email: diego.arosio@unimore.it

**L. Longoni · M. Papini · L. Zanzi**
Department of Civil and Environmental Engineering,
Politecnico di Milano,
Piazza Leonardo da Vinci 32, 20133, Milan, Italy

**G. Bièvre**
ISTerre,
Univ. Grenoble Alpes, Univ. Savoie Mont Blanc, CNRS, IRD, IFSTTAR,
ISTerre, 38000, Grenoble, France